
Imprint Reduction Using an Intensity Spike in OMEGA Cryogenic Targets

The primary obstacle to the successful implosion of an inertial confinement fusion target is hydrodynamic instability, which can cause the target to disintegrate and prevent it from reaching the high densities and temperatures required for ignition. The imploding target is primarily subject to the Rayleigh–Taylor (RT) instability, seeded by surface nonuniformity and by laser illumination nonuniformity, which can imprint itself on the target surface. Efforts to reduce laser imprint have employed primarily smoothing mechanisms such as smoothing by spectral dispersion (SSD),¹ distributed polarization rotators (DPR's),² and distributed phase plates (DPP's).³ We present here a novel technique to further reduce imprint in OMEGA cryogenic (cryo) targets by a relatively simple modification to the standard pulse shape.

As reported elsewhere in this volume (p. 49), the base-line OMEGA cryogenic targets consist of a shell of deuterium–tritium (DT) ice surrounding a DT vapor region. For target fabrication, the DT ice must be surrounded by a thin (1–4 μm) layer of plastic (CH) or polyimide. This layer increases, however, the amount of imprint by introducing an additional period of RT growth near the start of the laser pulse.⁴ Figure 82.9 shows the growth of laser imprint (i.e., the amplitude η of the outer-surface modulation) for a DT shell coated with 3 μm of CH, compared with the imprint that would result from a pure-DT shell. For this example, the target was illuminated with a 5% laser nonuniformity and a 50- μm nonuniformity wavelength. (To isolate the effect of laser nonuniformity, an initially smooth target surface was used in these simulations.) The qualitative features of the imprint are the same for both cases shown in Fig. 82.9. Initially, the imprint growth, which is roughly linear in time, results from the nonuniform shock, which is launched at the onset of laser irradiation. The imprint amplitude reaches a peak, representing the first quarter-cycle of the oscillations caused by dynamic overpressure.⁴ (For some wavelengths of nonuniformity, half the period of oscillation is less than the foot-pulse duration, and the outer-surface amplitude reverses phase.) The amplitude grows exponentially, after about 1.5 ns, as the whole shell begins to accelerate and RT growth sets in. During the drive pulse, the target with

the 3- μm CH shell has an imprint amplitude about twice that of the pure-DT shell. The increase in amplitude is initiated very early in the imprint process (within the first few hundred picoseconds for OMEGA targets), when a jump in the amplitude is produced by a brief acceleration of the CH shell, with resulting RT growth. The novel technique presented here significantly reduces this jump in amplitude and thereby reduces the imprint for the CH shell to approximately the level of the pure-DT shell.

The mechanism that produces the early, brief acceleration of the CH shell is illustrated in Fig. 82.10 by three plots of the density as a function of radius, at successive times early in the simulation. The onset of irradiation sends a shock into the CH layer. When the shock reaches the interface between the DT and the CH, a faster shock is sent into the less-dense DT, and a rarefaction wave (RW) returns to the outer surface through the CH layer. The RW accelerates the CH, while decreasing its pressure and density. While the outer surface is accelerated by the RW, it is subject to the RT instability.

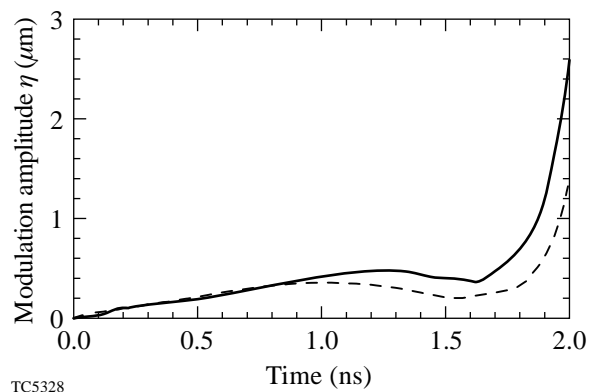


Figure 82.9

The amplitude of outer-surface modulations due to imprint, for an initially smooth target, driven by illumination with a 5%, 50- μm nonuniformity. The solid curve represents a target with a 3- μm CH layer surrounding a 72- μm DT ice shell, while the dashed curve represents 84 μm of DT, which gives the same total shell mass.

As the RW moves through the CH, it lowers the pressure from the post-shock CH pressure to the post-shock DT pressure; however, the laser irradiation imposes a pressure at the outer surface given by the ablation pressure. As a result, after the RW has crossed the outer surface, a weak *adjustment* shock is sent back into the target, which increases its pressure to the ablation pressure. This second shock is launched first at the trough of the surface perturbation, then later at the peak. This discrepancy in the time for the shock to be launched causes a decrease in the rate of amplitude growth $\dot{\eta}$.

The early-time growth due to the RW acceleration has the standard RT scaling and is greater for shorter wavelengths. For a given spherical harmonic with mode number ℓ , the corresponding wavelength for an OMEGA target is approximately three times smaller than for a NIF target, and as a result, the early-time growth is greater.

We have found a relatively simple way to reduce the increased imprint caused by the CH overcoat: By introducing a brief, high-intensity spike at the start of the foot pulse (see Fig. 82.11), the effects of the early-time acceleration of the CH shell can be drastically reduced. Figure 82.12 shows the degree of imprint (given by the outer-surface modulation amplitude) for identical targets, which have pulses with and without this intensity spike, for a 50- μm illumination perturbation. The spike, which is 50 ps in duration and has an intensity ratio with

the foot of 6:1, reduces the imprint by ~ 2 at this wavelength. As seen, targets irradiated with an initial intensity spike experience a shorter period of early RT growth, which begins earlier in time, than those irradiated by the standard pulse. As a result, the RT growth starts with a lower amplitude and terminates earlier.

The intensity spike launches a stronger shock than the canonical foot-pulse shock. This results in a larger shock velocity, a greater amount of compression, and a thinner post-shock CH layer. Thus, the shock reaches the CH–DT interface earlier, and the rarefaction wave returns more quickly because of the thinner post-shock CH layer. (A stronger shock also leads to a greater post-shock temperature and higher sound speed, so that the RW travels more quickly.) This decreases not only the arrival time of the rarefaction wave but also its extent since the width of the RW grows linearly in time. As shown in Appendix A, the duration of the RT growth due to the RW is proportional to $d/(\xi c_s)$, where d is the width of the CH layer, ξ is the amount of shock compression, and c_s is the post-shock sound speed. As this dependence suggests, both of these factors lead to less early-time RT growth and less imprint.

For OMEGA cryo targets, the most-unstable modes are commonly taken to have spherical-harmonic mode numbers in the range $20 \leq \ell \leq 75$ (corresponding to illumination nonuniformity wavelengths of $40 \mu\text{m} \leq \lambda \leq 140 \mu\text{m}$). RT

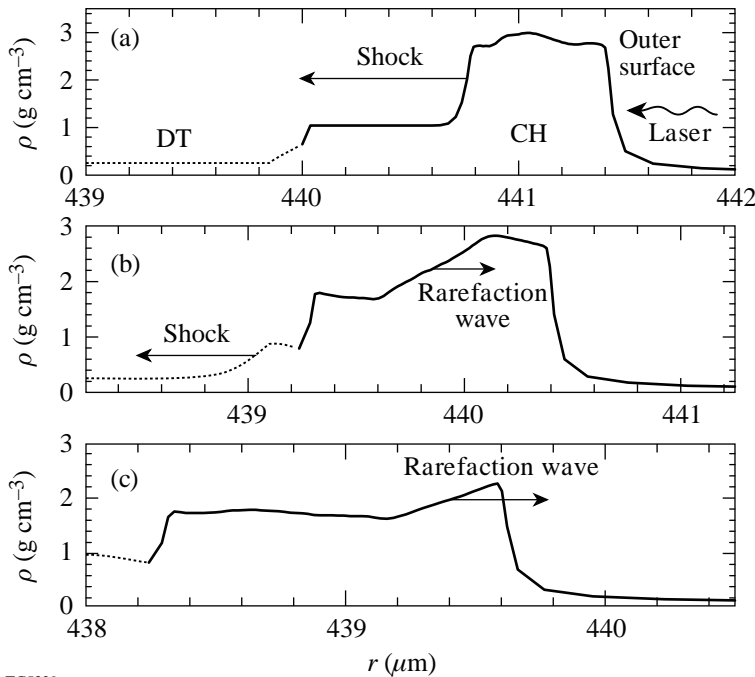
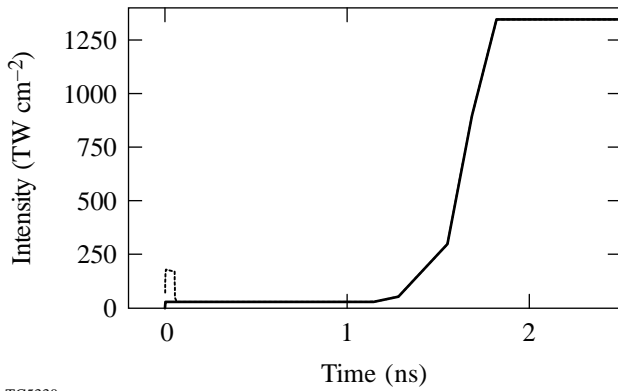


Figure 82.10
The density profile at the outer edge of the target shell is shown at three consecutive times early in the implosion. Panel (a) shows the propagation of the foot-pulse shock through the thin outer CH layer. Panel (b) shows the return of the rarefaction wave from the CH/DT interface through the shocked CH to the outer surface of the target. Panel (c) shows the density while the rarefaction wave is accelerating the outer surface to the post-shock speed of the shocked DT. The CH layer is shown with a solid line, and the DT ice is represented by a dotted line.

TC5329

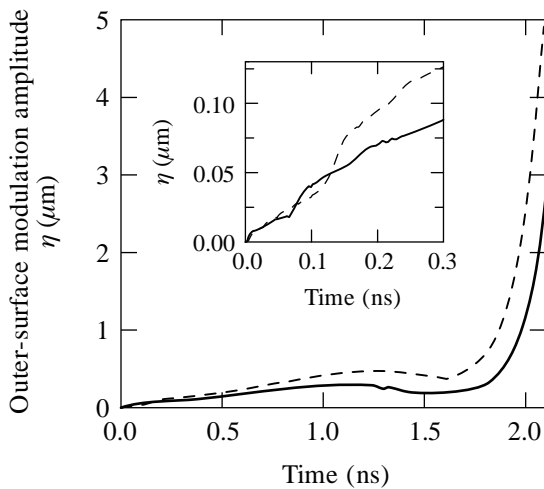
growth is greater for shorter wavelengths. Figure 82.13 shows pairs of simulations, with (solid) and without (dashed) the intensity spike, for two wavelengths, demonstrating this wavelength dependence.

A direct measure of the magnitude of imprint was suggested in Ref. 5 by Weber *et al.* They evaluate the degree of imprint by calculating, for a given illumination nonuniformity of wave number k , the *equivalent surface finish* $\varepsilon(k)$, defined as the



TC5330

Figure 82.11
The pulse shape of an OMEGA cryogenic target, with (dotted) and without (solid) the initial intensity spike.



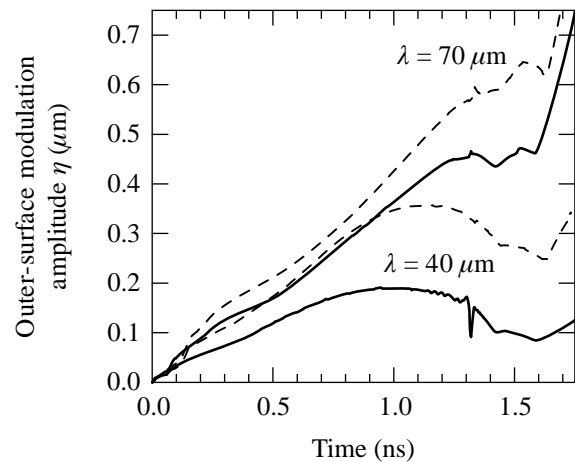
TC5331

Figure 82.12
The amplitude η of the outer-surface modulation is shown for a 50- μm -wavelength illumination perturbation, for targets using a 3- μm overcoat layer of CH. The simulation using the standard cryo laser pulse is shown by a dashed line, while the simulation that used an initial intensity spike is shown by a solid line. The spike reduces the imprint by a factor of ~ 2 at this wavelength. The early-time behavior is shown in the inset.

magnitude of initial surface nonuniformity $\eta_{\text{surface}}(k, t = 0)$ necessary, in the absence of illumination nonuniformity, to produce the same outer-surface modulation amplitude $\eta_{\text{surface}}(k, t)$ during the drive pulse:

$$\varepsilon(k) \equiv \frac{\eta_{\text{imprint}}(k, t)}{\eta_{\text{surface}}(k, t)} \eta_{\text{surface}}(k, t = 0). \quad (1)$$

Figure 82.14 shows the equivalent surface finish as a function of mode number ℓ for simulations with and without the intensity spike, compared with that of an all-DT target with the standard pulse. In all cases (except for the short-wavelength, all-DT simulations, not shown in the figure), the spike reduces imprint. The equivalent surface finish was computed using the growth formula of Betti *et al.*,⁶ where the ablation velocity, density scale length, and acceleration were taken from the all-DT, no-spike simulation, with coefficients $\alpha = 0.94$ and $\beta = 2.6$ during DT ablation and $\alpha = 1.0$ and $\beta = 1.7$ during CH ablation. We have also found that the thicker the outer CH layer, the greater the imprint reduction. The reduction in equivalent surface finish is large enough that even a target with a 3- μm outer CH layer has the same equivalent surface finish as an all-DT target. This is also shown in Table 82.II, which lists the equivalent surface finish, averaged over mode number ℓ , for a range of CH-layer thicknesses.



TC5332

Figure 82.13
The outer-surface modulation amplitude η , for an initially smooth target, for a range of illumination nonuniformity wavelengths λ . Simulations are of targets with a 3- μm outer layer of CH. Pulses with (without) the intensity spike are shown with solid (dashed) lines.

The initial intensity spike reduces imprint primarily by reducing the early-time RT growth resulting from the CH layer that overcoats the DT shell. Even for a single-layer target, however, the period of increased intensity further reduces imprint by increasing the size of the plasma atmosphere around the target. The laser energy is deposited primarily outside the critical surface in the target’s corona, where the plasma frequency equals the laser light’s frequency. This energy is conducted thermally to the ablation surface. Modeling the conduction zone has shown that the pressure perturbation decreases exponentially with distance from the critical surface,⁷ so

$$\tilde{p}_a/p_a \sim (\tilde{I}/I) \exp(-fkD_c),$$

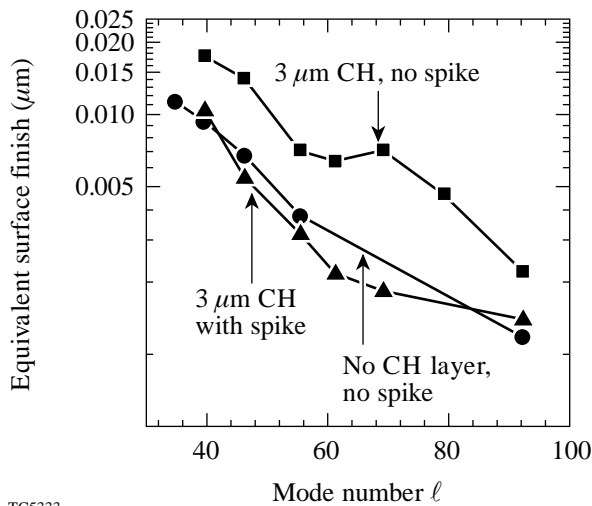
where D_c is the distance between the critical and ablation surfaces, or *smoothing distance*, p_a is the ablation pressure, \tilde{p}_a is its modulation amplitude, I is the laser intensity, \tilde{I} its modulation amplitude, and f is of order unity. The smoothing distance increases linearly in time, so $D_c \sim V_c t$, where V_c is the velocity of the critical surface with respect to the ablation surface. Greater laser intensity results in a more rapid growth of the conduction zone and a larger V_c . Analytical modeling of the conduction zone⁸ shows a scaling of $D_c \sim I^{4/3}$. Once $kD_c \sim 1$, at the *decoupling time*, the laser nonuniformities are

decoupled from the target surface, and the ablation pressure is essentially uniform.

Because the degree of thermal smoothing is greater for higher laser intensities, the initial intensity spike also reduces imprint by increasing the smoothing distance. A series of simulations were performed for different wavelengths, with and without an intensity spike, of a target consisting of a shell of 84 μm of DT ice. This shell width was chosen so the total shell mass would be comparable to that of the simulations with

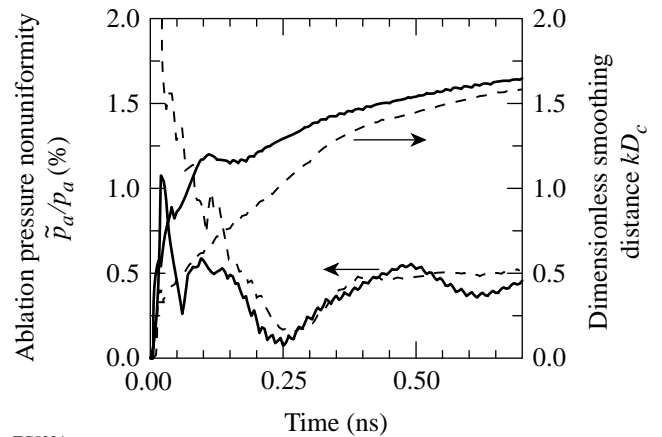
Table 82.II: The approximate reduction factor in equivalent surface finish, averaged over mode number ℓ , $\langle \epsilon/\epsilon_{\text{spike}} \rangle_\ell$, is shown for various thicknesses d (in μm) of the outer CH layer. Also shown is $\langle \epsilon_{\text{spike}}/\epsilon_{\text{DT}} \rangle_\ell$, the approximate average over mode number of the ratio of equivalent surface finish for a simulation with an intensity spike and d microns of CH, to that of an all-DT target, without the intensity spike.

d (μm)	$\langle \epsilon/\epsilon_{\text{spike}} \rangle_\ell$	$\langle \epsilon_{\text{spike}}/\epsilon_{\text{DT}} \rangle_\ell$
0	1.2	2.40
1	1.7	0.80
2	1.9	1.00
3	2.7	0.76



TC5333

Figure 82.14 The equivalent surface finish for a series of mode numbers ℓ , for simulations with a 3- μm outer CH layer, with and without an initial intensity spike, and for a pure-DT target without an intensity spike.



TC5334

Figure 82.15 The ablation pressure nonuniformity \tilde{p}_a/p_a and dimensionless smoothing distance kD_c for simulations with (solid) and without (dashed) an initial intensity spike. For these simulations, $\lambda = 50 \mu\text{m}$. The smoothing distance is taken to be the distance from the ablation surface to the critical surface. The curves showing \tilde{p}_a/p_a have been smoothed numerically to reduce the noise due to finite simulation resolution.

a 3- μm CH layer, which have 72 μm of DT. Consider first the simulation with $\lambda = 50 \mu\text{m}$: From the slope of $\eta(t)$ in Fig. 82.15, which shows the ablation pressure nonuniformity \tilde{p}_a/p_a and dimensionless smoothing distance kD_c for simulations with (solid) and without (dashed) an initial intensity spike, we see that for the standard pulse shape, $V_c \sim 35 \mu\text{m ns}^{-1}$ (ignoring the zero-time offset). This means that the decoupling time $t_c \sim 230$ ps. Figure 82.15 also shows that, for $t \geq t_c$, the ablation pressure nonuniformity \tilde{p}_a/p_a has decreased to its asymptotic foot-pulse value of $\sim 0.4\%$. By contrast, the simulation (represented by the solid line) with the spike has a decoupling velocity, during the first 100 ps, of $V_c \approx 90 \mu\text{m ns}^{-1}$, and a correspondingly smaller decoupling time and ablation-pressure nonuniformity. In this case, the decoupling speed V_c decreases at $t \sim 100$ ps because of the decrease in the laser intensity. The outer-surface modulation amplitude is shown in Fig. 82.16 (solid curves for pulse shapes including the intensity spike). As described above, η initially grows linearly. For example, the 50- μm simulation without the spike has a perturbed shock speed of $\tilde{v}_s \approx 0.7 \mu\text{m ns}^{-1}$, which produces a linear growth rate of $\dot{\eta} = 0.52 \mu\text{m ns}^{-1}$ (see Appendix A). This is comparable to the growth rate shown in Fig. 82.16.

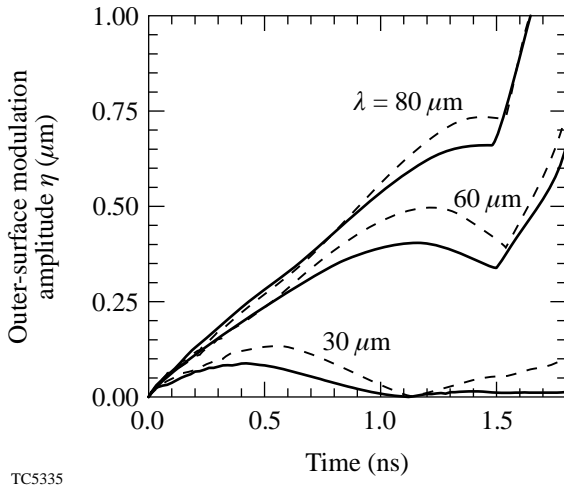


Figure 82.16
The amplitude of the outer-surface modulation for various illumination nonuniformity wavelengths, for targets without a CH overcoat. Dashed curves represent the standard OMEGA cryogenic pulse shape, while the solid curves represent pulses with an initial intensity spike.

To facilitate modeling, an intensity spike with a sharp rise and fall was used for the simulations described above. A realistic pulse will have a finite rise and fall time. Replacing the square spike profile with a Gaussian profile preserves the essential features and imprint reduction described above: For

$\lambda = 50 \mu\text{m}$, and a 5% laser nonuniformity amplitude, the equivalent surface finish for a 50-ps, 180-TW cm^{-2} spike is 0.0032 μm , while for a 50-ps FWHM Gaussian spike with a peak intensity of 200 TW cm^{-2} (which delivers roughly the same energy), it is 0.003 μm . (This is to be compared with an equivalent surface finish of 0.007 μm without the intensity spike.) For a longer, less-intense spike of 100 ps and 120 TW cm^{-2} , the equivalent surface finish is 0.00055 μm , while for a 100-ps FWHM Gaussian spike with a peak intensity of 140 TW cm^{-2} , it is 0.001 μm .

The performance of an OMEGA target is reflected by the neutron yield Y that it produces. For an OMEGA cryo target, the drive-pulse shock must be launched sufficiently after the weaker foot-pulse shock so that they break out of the main fuel layer at about the same time. A change in the initial intensity changes the shock speed, potentially altering the shock timing. The fractional neutron yield (relative to the yield with no spike) for a range of intensity spike durations (dt) and intensities (I) is shown in Fig. 82.17. As this figure shows, the greater the I or dt , the lower the yield. However, because the foot pulse does not maintain the intensity used in the spike, the shock is unsupported and, after the duration of the spike, evolves into a decaying N -wave.⁹ The true measure of the disruption caused by the spike is the energy it delivers to the target, $I dt$, as shown by the contours of constant Y in Fig. 82.17. Based on the 1-D

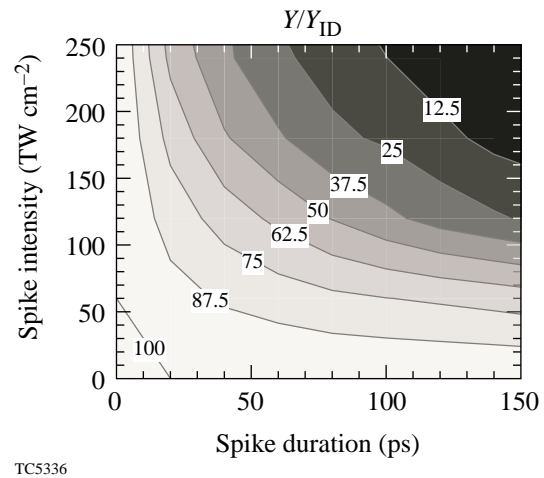


Figure 82.17
Neutron yield as a fraction of the yield with no intensity spike, plotted in terms of the spike duration dt and intensity I . A spike intensity of less than the foot-pulse intensity, or duration of zero, indicates that the spike is absent. Operating on the 80% contour line will reduce imprint by about a factor of 2. Much of the reduction in yield can be recovered by shortening the foot pulse. Yields were calculated with *LILAC*.

simulations, the yield $Y(I, dt)$ is of the same order as that of the canonical cryo target for a wide range of spike intensities and durations. In addition, because $I dt \ll I_{\text{foot}} dt_{\text{foot}}$, the fuel adiabat α and the RT growth factor are not significantly changed by the spike. The main effect of the intensity spike is to alter the shock timing. For the example of a 100-ps spike with twice the foot-pulse intensity (i.e., 60 TW cm^{-2}), the imprint reduction is approximately a factor of 2 and the decrease in 1-D yield is only 20%. Much of the reduction in yield shown in Fig. 82.17 may be recovered by slightly shortening the duration of the foot pulse.

In summary, the presence of an initial intensity spike at the start of the foot pulse in an OMEGA cryogenic target reduces imprint by about a factor of 2 for typical target configurations. This imprint reduction comes at the cost of only a modest decrease in yield, most of which can be recovered by a small reduction in pulse length. Furthermore, this reduction in imprint occurs for those wavelengths of illumination nonuniformity considered to be the most dangerous for target performance.

ACKNOWLEDGMENT

One of the authors (TJBC) would like to thank V. Goncharov and P. B. Radha for many useful discussions. This work was supported by the U.S. Department of Energy Office of Inertial Confinement Fusion under Cooperative Agreement No. DE-FC03-92SF19460, the University of Rochester, and the New York State Energy Research and Development Authority. The support of DOE does not constitute an endorsement by DOE of the views expressed in this article.

Appendix A: Rarefaction-Wave Rayleigh–Taylor Growth

The RT growth due to the early-time RW acceleration was first discussed in the context of feedout by Betti *et al.*¹⁰ A simple estimate of the early-time RT growth for NIF targets was performed by Goncharov *et al.*¹¹ using scaling laws. In this appendix we approximate the period of RT growth due to the RW return from the DT/CH interface in OMEGA cryo targets. As discussed above, when the foot shock reaches the interface between the CH and the DT ice, it behaves as if it has reached a contact discontinuity. At this point it proceeds as a stronger shock into the DT and sends a rarefaction wave outward toward the outer surface, communicating the new post-shock conditions. When the RW crosses the outer surface, it is accelerated to the post-shock speed of the DT.

This process is shown in Fig. 82.18, an $r-t$ diagram for a simulation with a $72\text{-}\mu\text{m}$ shell of DT ice, surrounded by $3\text{-}\mu\text{m}$ of CH, and the standard OMEGA cryo pulse shape (see Fig. 82.11). (This DT-shell width was chosen so the shell would have the same total mass as that of the all-DT simula-

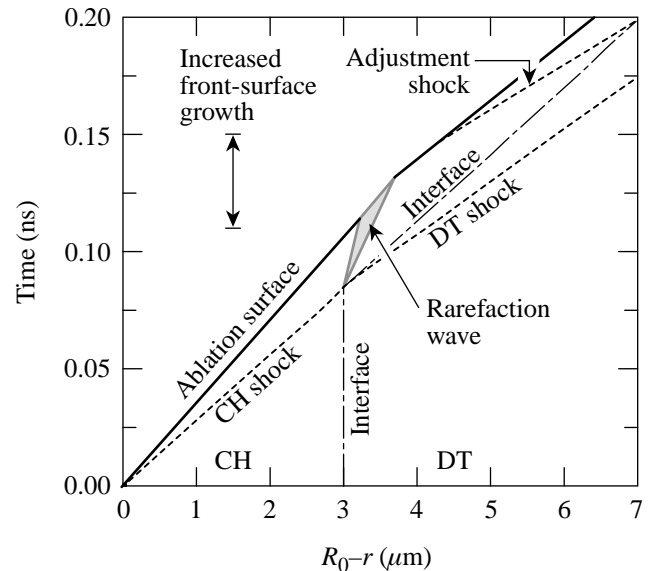
tions.) The duration of the RT growth may be estimated as follows: the RW is launched from the point (r_0, t_0) , where $r_0 = R_0 - d$ ($d = 3\text{-}\mu\text{m}$ being the width of the CH layer) and $t_0 = r_0/v_s$ (v_s being the shock speed). The outer edge of the RW travels at the post-CH-shock sound speed, while the inner edge travels with a velocity of v_{RW} , given in Ref. 9 as

$$v_{\text{RW}} = -c_s + \frac{1}{2} [(\gamma + 1)V - (\gamma - 1)u]. \quad (\text{A1})$$

Here V is the post-DT-shock speed, γ is the ratio of specific heats, and $u = (1 - \xi^{-1})v_s$ is the post-shock speed, where ξ is the degree of shock compression and a strong shock is assumed. The intersection (r_1, t_1) of the ablation front, which travels at speed u , and the outer edge of the RW wave is given by

$$r_1 = R_0 - d(1 - \xi^{-1})(1 + \xi^{-1}M_{\text{CH}}), \quad (\text{A2})$$

$$t_1 = \frac{d}{v_s}(1 + \xi^{-1}M_{\text{CH}}), \quad (\text{A3})$$



TC5337

Figure 82.18

An $r-t$ diagram for an OMEGA cryo simulation with a $50\text{-}\mu\text{m}$ illumination perturbation, and a target shell composed of $72\text{-}\mu\text{m}$ of DT ice and $3\text{-}\mu\text{m}$ of CH. Shock and interface trajectories are shown as functions of the time t and the distance $R_0 - r$ from the initial outer radius R_0 . Note that, when the foot-pulse shock reaches the DT/CH interface, the shock speed increases and a forward-swept rarefaction wave (shaded region) is launched. Because the post-DT-shock pressure is not equal to the ablation pressure, a second adjustment shock is sent into the shell. Shocks are represented by dashed lines, and the CH/DT interface by a dashed-dotted line.

where M_{CH} is the Mach number of the foot-pulse shock traveling through the CH. If we approximate the speed of the ablation front during its passage through the RW by the average between its speeds before and after, $(u + V)/2$, the duration Δt of the RW acceleration is given by

$$\Delta t \approx \frac{(\gamma + 1) [\xi M_{\text{DT}} - (\xi - 1) M_{\text{CH}}]}{\{2\xi - \gamma [\xi M_{\text{DT}} - (\xi - 1) M_{\text{CH}}]\}} \times \frac{d}{\xi c_s}, \quad (\text{A4})$$

where $M_{\text{DT}} \equiv V/c_s$. During this period, the ablation surface is subject to the RT instability. In addition, because the RW reaches the “trough” of the outer-surface perturbation first, the period of acceleration is extended by a period of approximately $\Delta t' = 2|\eta(t_1)|/c_s$. For uniform laser illumination, the outer radius of the target is given, during the foot pulse (and before foot-pulse shock breakout), by $R(t) = R(0) - ut = R(0) - (1 - \xi^{-1})v_s t$, where t is the time since the start of the laser pulse and u is the post-shock speed. Perturbing this equation for $R(t)$, we find that an initially smooth target will develop a surface modulation given by

$$\eta(t) = (1 - \xi^{-1}) \tilde{v}_s t, \quad (\text{A5})$$

where \tilde{v}_s is the modulation amplitude of the shock speed, assuming a strong shock. Inserting Eq. (A5) into the expression for $\Delta t'$ yields

$$\Delta t' \approx 2 \frac{d}{c_s} (1 - \xi^{-1}) (1 + M_{\text{CH}} \xi^{-1}) \frac{\tilde{M}_{\text{CH}}}{M_{\text{CH}}}, \quad (\text{A6})$$

where $\tilde{M}_{\text{CH}} \equiv \tilde{v}_s/c_s$. The RT growth factor due to the RW is given approximately by

$$G_{\text{RW}} \approx e^{\sqrt{(V-u)k(\Delta t + \Delta t')}}. \quad (\text{A7})$$

After the early period of growth, the outer-surface modulation continues to grow at a constant rate. As the RW propagates, it lowers the pressure and density of the shocked CH; however, as mentioned above, the laser imposes a pressure equal to the

ablation pressure at the outer surface. Thus when the RW reaches the outer surface, a second, *adjustment* shock is launched into the CH to increase the pressure in the shell. As this shock is launched, $\dot{\eta}$ is decreased to approximately the value it had before the RW return. The inset in Fig. 82.12 shows the period of initial linear growth, followed by the early-time RT growth. There is a subsequent decrease in the linear growth rate because the adjustment shock is launched from the trough of the surface perturbation before the peak. The outer surface undergoes slightly more than one quarter of a period of an oscillation before the drive pulse begins, followed by RT growth.

REFERENCES

1. S. Skupsky, R. W. Short, T. Kessler, R. S. Craxton, S. Letzring, and J. M. Soures, *J. Appl. Phys.* **66**, 3456 (1989).
2. T. R. Boehly, V. A. Smalyuk, D. D. Meyerhofer, J. P. Knauer, D. K. Bradley, C. P. Verdon, and D. Kalantar, in *Laser Interaction and Related Plasma Phenomena*, edited by G. H. Miley and E. M. Campbell (American Institute of Physics, New York, 1997), Vol. 406, pp. 122–129.
3. Y. Lin, T. J. Kessler, and G. N. Lawrence, *Opt. Lett.* **20**, 764 (1995).
4. Laboratory for Laser Energetics LLE Review **80**, 185, NTIS document No. DOE/SF/19460-321 (1999). Copies may be obtained from the National Technical Information Service, Springfield, VA 22161.
5. S. V. Weber, S. G. Glendinning, D. H. Kalantar, M. H. Key, B. A. Remington, J. E. Rothenberg, E. Wolfrum, C. P. Verdon, and J. P. Knauer, *Phys. Plasmas* **4**, 1978 (1997).
6. R. Betti, V. N. Goncharov, R. L. McCrory, P. Sorotokin, and C. P. Verdon, *Phys. Plasmas* **3**, 2122 (1996).
7. K. A. Brueckner and S. Jorna, *Rev. Mod. Phys.* **46**, 325 (1974).
8. W. M. Manheimer, D. G. Colombant, and J. H. Gardner, *Phys. Fluids* **25**, 1644 (1982).
9. G. B. Whitham, *Linear and Nonlinear Waves*, Pure and Applied Mathematics (Wiley, New York, 1974).
10. R. Betti, V. Lobatchev, and R. L. McCrory, *Phys. Rev. Lett.* **81**, 5560 (1998).
11. V. N. Goncharov, S. Skupsky, T. R. Boehly, J. P. Knauer, P. McKenty, V. A. Smalyuk, R. P. J. Town, O. V. Gotchev, R. Betti, and D. D. Meyerhofer, *Phys. Plasmas* **7**, 2062 (2000).